1452 *Chem. Mater.* **2010,** *22,* 1452–1461
DOI:10.1021/cm902957r

CHEMISTRY OF MATERIALS
Article

Defect Structure, Charge Transport Mechanisms, and Strain Effects in $Sr_4Fe_6O_{12+\delta}$ Epitaxial Thin Films

Cecilia Solís,[†,§] WooChul Jung,[‡] Harry. L. Tuller,[‡] and José Santiso*,[†]

[†]*Centro de Investigación en Nanociencia y Nanotecnologia, CIN2* (*CSIC-ICN*), *Campus UAB, 08193 Bellaterra, Barcelona, Spain and* [‡]*Department of Materials Science and Engineering, MIT, Cambridge, Massachusetts 02139 .* [§] *Present address: Instituto de Tecnología química* (*CSIC-Univ. Politécnica de Valencia*), *Av. de los Naranjos, s/n, Valencia E-46022, Spain.*

Received September 23, 2009. Revised Manuscript Received December 16, 2009

The defect structure and charge transport mechanisms of layered perovskite-related structure $Sr_4Fe_6O_{12+\delta}$ in the form of epitaxial thin films are studied as a function of temperature, oxygen partial pressure, and the type of substrate upon which they were grown. Values for the band gap, oxidation, and reduction enthalpies are extracted by fitting the experimental data to a defect model assuming a high oxygen deficiency. The electrical conductivity was dominated by *p*-type and *n*-type electronic conductivity at high and low oxygen partial pressures, respectively, with no evidence of a measurable ionic conductivity. Specimens cooled to below 400 °C after being annealed at different pO_2's at elevated temperatures exhibited an activated conductivity whose activation energy E_a increased from ~0.2 eV to ~1.0 eV as the pO_2 at which the specimens were annealed decreased from 1 atm to 10^{-4} atm. These data, which are also examined with respect to the different epitaxial strains induced by selecting substrates with different lattice mismatches, are analyzed in terms of a small-polaron hopping mechanism. Subtle structure modulations, induced in the films by increasing epitaxial strain, are shown to be capable of modifying the intrinsic transport mechanisms in $Sr_4Fe_6O_{12+\delta}$ and enhancing the electronic conductivity by an order of magnitude.

Introduction

Research in complex oxides with layered structures is gaining interest among the solid state ionics research community because of the outstanding mixed ionic-electronic conductivities of some perovskite-related structure transition-metal oxides, such as cobaltites,[1,2] nickelates,[3,4] or ferrites.[5−7] This makes them attractive candidates for improving the performance of electrochemical devices as cathodes for solid oxide fuel cells[1,8] or as active layers in resistive gas sensors.[9,10] The layered structure of these compounds often results in transport properties that are highly anisotropic. Thin epitaxial films therefore enable the study of charge transport along specific crystallographic directions, thus offering better insight into the nature of the anisotropy. Furthermore, significant levels of strain induced in thin films by epitaxial growth on mismatched substrates offer the possibility of studying the role that subtle structural changes can have on transport mechanisms.

Studies of the high temperature electrical conductivity of these materials, at different temperatures, and particularly at different oxygen partial pressures, can contribute meaningful information about the defect equilibrium and ionic-electronic transport mechanisms. Among complex oxides, perovskite-related iron oxides, such as $SrFe_xTi_{1-x}O_3$, have been the subject of detailed studies concerning their high-temperature electronic transport properties.[11] Recent structural studies on one of these layered iron oxides, $Sr_4Fe_6O_{12+\delta}$, have revealed the appearance of a modulated structure showing subtle variations induced by oxygen stoichiometry and strain variations in epitaxial films,[12,13] thereby illustrating the complexity that some layered compounds may reach. Figure 1 shows a scheme of the $Sr_4Fe_6O_{12+\delta}$ structure with $\delta = 0.8$. $Sr_4Fe_6O_{12+\delta}$ presents an intergrowth structure, which consists of an alternating stack along the *b* axis (vertical direction in the figure) of $SrFeO_3$ perovskite-type layers,

*Corresponding author fax: +34 935813717; e-mail: jsantiso@cin2.es.

(1) Skinner, S. J. *Int. J. Inorg. Mater.* **2001**, *3*, 113–121.
(2) Yasumoto, K.; Inagaki, Y.; Shiono, M.; Dokiya, M. *Solid State Ionics* **2002**, *148*, 545–549.
(3) Kharton, V. V.; Viskup, A. P.; Kovalevsky, A. V.; Naumovich, E. N.; Marques, F. M. B. *Solid State Ionics* **2001**, *143*, 337–353.
(4) Boehm, E.; Bassat, J.-M.; Dordor, P.; Mauvy, F.; Grenier, J.-C.; Stevens., Ph. *Solid State Ionics* **2005**, *176*, 2717–2725.
(5) Mai, A.; Haanappel, V. A. C.; Uhlenbruck, S.; Tietz, F.; Stover, D. *Solid State Ionics* **2005**, *176*, 1341–1350.
(6) Simner, S. P.; Bonnett, J. R.; Canfield, N. L.; Meinhardt, K. D.; Shelton, J. P.; Sprenkle, V. L.; Stevenson, J. W. *J. Power Sources* **2003**, *113*, 1–10.
(7) Orui, H.; Watanabe, K.; Arakawa, M. *Electrochem. Soc. Proc. SOFC VIII* **2003**, *07*, 571–579.
(8) Maguire, E.; Gharbage, B.; Marques, F. M. B.; Labrincha, J. A. *Solid State Ionics* **2000**, *127*, 329–335.
(9) Fergus, J. W. *Sens. Actuators, B* **2007**, *123*, 1169–1179.
(10) Rothschild, A.; Tuller, H. L. *J. Electroceram.* **2006**, *17*, 1005–1012.
(11) Rothschild, A.; Menesklou, W.; Tuller, H. L.; Ivers-Tiffee, E. *Chem. Mater.* **2006**, *18*, 3651–3659.
(12) Santiso, J.; Pardo, J. A.; Solís, C.; Garcia, G.; Figueras, A.; Rossell, M. D.; Van Tendeloo, G. *Appl. Phys. Lett.* **2005**, *86*, 132105.
(13) Solís, C.; Rossell, M .D.; Garcia, G.; Van Tendeloo, G.; Santiso, J. *Adv. Funct. Mater.* **2008**, *18*, 785–793.

 Published on Web 01/08/2010

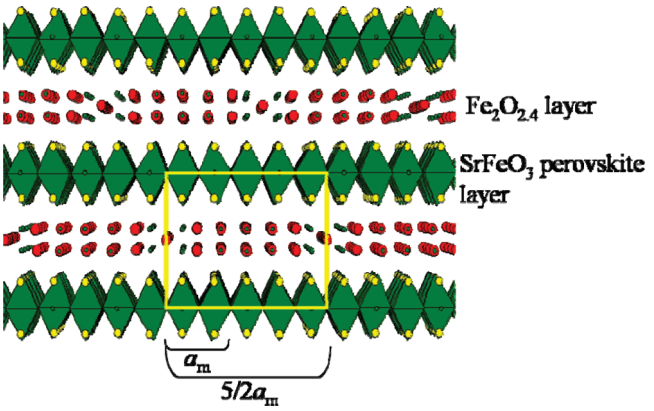

Figure 1. Scheme of the $Sr_4Fe_6O_{12+2\alpha}$ structure with modulation vector $\alpha = 2/5$ ($Sr_4Fe_6O_{12.8}$). It corresponds to a modulation taking place each five Fe−O octahedral units along the *a* axis of the structure.

with Fe−O coordinated octahedra, and $Fe_2O_{2+\delta/2}$ double layers of five-coordinated iron polyhedra. The variable oxygen stoichiometry δ of the $Fe_2O_{2+\delta/2}$ layers consists of additional single oxygen rows that arrange periodically along the *a* axis of the structure (horizontal in the figure) inducing a modulated structure. The modulation is often described in terms of a modulation vector $\boldsymbol{q} = \alpha \boldsymbol{a}_m$, in the reciprocal space, related to the periodicity of the parent structure with vector $\boldsymbol{a}_m$ (that in real space corresponds to a periodicity every two Fe−O octahedral, as it is shown in the figure) times a parameter α that describes each particular modulation. For a commensurate structure, the modulation shows a long-range order and corresponds to an integer number of octahedra units. The figure shows, as an example, one of these cases with a modulation periodicity each 5 octahedra, than corresponds to $\alpha = 2/5$. One can easily imagine more complex situations where there is a combination of different arrangements along the *a* axis giving place to an average modulation with noninteger values of octahedral units, so the α modulation parameter can show a continuous range of values. Therefore the composition of the double layers is $Fe_2O_{2+\alpha}$, and thus, $Sr_4Fe_6O_{12+2\alpha}$. The present study will analyze how the modulation parameter α is implicated in the charge transport properties.

In these type of semiconducting metal oxide compounds, it is generally assumed that charge transport takes place via a thermally activated small-polaron hopping mechanism.[14,15] Taking into account the Emin-Holstein model for the adiabatic approximation,[16] the temperature dependence of the conductivity follows the expression

$$\sigma(T) = (A/T)\exp(-E_a/kT) \qquad (1)$$

with *k* representing the Boltzmann constant, and E_a and A, the activation energy and preexponential factor , respectively. The activation energy E_a and the preexponential factor *A*, in turn, depend on the convolution of carrier mobility and concentration.

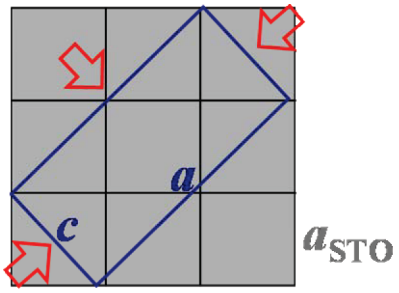

Figure 2. Planar view of the alignment of the $Sr_4Fe_6O_{13}$ *a*-*c* plane of the film on to the $SrTiO_3$(001) plane of the substrate. The arrows indicate the expected compressive strain induced in the film by the substrate mismatch.

In the present work, the planar conductivity of $Sr_4Fe_6O_{12+\delta}$ epitaxial films, deposited on different perovskite substrates ($NdGaO_3$, $SrTiO_3$, and $LaAlO_3$), was studied over a wide range of oxygen partial pressures (pO_2) and temperatures. Changes in E_a as well as in *A* are related to changes in oxygen stoichiometry, strain, and structural modulation. The results demonstrate that epitaxial strain may serve as a tool for modifying charge transport mechanisms in thin films.

Experimental Section

High quality epitaxial *b*-axis oriented $Sr_4Fe_6O_{12+\delta}$ thin films, with thickness ranging from 5 to 300 nm, were deposited onto (100) $SrTiO_3$ (STO), (110) $NdGaO_3$ (NGO), and (012) $LaAlO_3$ (LAO) substrates by pulsed laser deposition at 750 °C and 1 Pa of oxygen pressure, as described in previous work.[17,18] The structure for $Sr_4Fe_6O_{13}$ as first reported by Yoshiasa et al.[19] has cell parameters $a = 1.1103$, $b = 1.8924$, and $c = 0.5572$ nm. There is an obvious close matching between *a*-*c* planes of the structure and the (100) planes of any cubic perovskite structure because their planes consist of the same octahedra arrangement (as it was described in previously). This does not happen in any other plane of the structure. Therefore we can expect an epitaxial arrangement of both structures in such a way that their corresponding octahedral units lie parallel on top of each other, as it is depicted in Figure 2. The $Sr_4Fe_6O_{12+\delta}$ films grow on the different substrates as follows. STO is cubic perovskite with $a = 0.3905$ nm. If we consider *a* and *c* parallel to the [110] direction of the substrate, the films grow on the substrates by adjusting $a/2$ and *c* parameters of the films to $\sqrt{2}a$STO (0.552 nm). This gives rise to a mismatch of −0.52% and −0.89% along *a* and *c* axis. NGO is an orthorhombic perovskite with $a = 0.5424$ nm, $b = 0.5501$ nm, and $c = 0.7701$ nm, so the (110) plane is equivalent to *a* (001) plane of a cubic perovskite and defines a rectangular plane with parameters $a_c = 0.3863$ nm and $b_c = 0.3854$ nm. The films will grow on the (110) planes of NGO substrates by adjusting $a/2$ and *c* parameters to the a_c and b_c parameters of the substrate. This gives a mismatch of about −1.8% and −2.0%, respectively (slightly larger than on STO substrate). LAO is a trigonal perovskite which can be described

(14) Patrakeev, M. V.; Leonidov, I. A.; Kozhevnikov, V. L.; Kharton, V. V. *Solid State Sci.* **2004**, *6*, 907–913.
(15) Mogni, L.; Fouletier, J.; Prado, F.; Caneiro, A. *J. Solid State Chem.* **2005**, *178*, 2715–2723.
(16) Emin, D.; Holstein, T. *Ann. Phys.-New York* **1969**, *53*, 439.
(17) Rossell, M. D.; Abakumov, A. M.; Van Tendeloo, G.; Pardo, J. A.; Santiso, J. *Chem. Mater.* **2004**, *16*, 2578–2584.
(18) Pardo, J. A.; Santiso, J.; Solís, C.; Garcia, G.; Figueras, A.; Rossell, M. D.; Van Tendeloo, G. *J. Cryst. Growth* **2004**, *262*, 334–340.
(19) Yoshiasa, A.; Ueno, K.; Kanamaru, F.; Horiuchi, H. *Mater. Res. Bull.* **1986**, *21*, 175.

as a distorted perovskite with $a = c = 0.3789$ nm and $\alpha = \beta = \gamma = 90.12°$. The (012) plane of this structure corresponds to the (001) primitive perovskite cell, with an equivalent pseudocubic cell parameter of $a = 0.3789$ nm. Therefore the films grown on the (012) planes of LAO substrates give rise to a mismatch of −3.6% (larger than STO and NGO). The negative sign of the mismatch on all the considered substrates indicates that film has a larger parameter than the substrates, so the films will have a tendency to present an in-plane biaxial compressive strain when grown epitaxially on these substrates.

The measured values of the cell parameters after film deposition have shown that thinner films of about 10−20 nm on STO and NGO substrates are almost fully strained, and upon thickness increase above a certain critical thickness (not precisely defined, but might be closer to 20−30 nm) the strain progressively reduces approaching expected bulk values. This is the expected behavior of any defect-mediated strain relaxation mechanism. Films on LAO have shown already cell parameter values closer to the bulk ones even for the thinner films. This is due to the larger mismatch between $Sr_4Fe_6O_{13}$ and LAO substrate (about −3.6%) which reduces the corresponding critical thickness for a fully strained epitaxial growth to a value below the explored range. Therefore all the films grown on LAO correspond already to a fully relaxed structure. More details about the relaxation mechanism upon thickness increase, and the way this is related to the variations in the modulated structure can be found in ref 13.

The thickness of the films, up to 100 nm, was measured by X-ray reflectometry, while for thicker samples, values were extrapolated from the growth rate determined for the thin films.

The strain in the films was calculated from the difference in the cell parameters measured at a given thickness (the out-of-plane b parameter was calculated by XRD from the 2θ angular positions of different $0k0$ reflections) and those of the asymptotic tendency at larger thicknesses (taken as the equilibrium structure). The corresponding oxygen modulation parameter α for each film (as described in the Introduction) was extracted from the angular positions of different $hk0$ (k = odd) asymmetric reflections in the reciprocal space maps, measured by means of an X-ray Philips MRD diffractometer equipped with a four-angle goniometer and parallel beam optics. [12]

The planar measurements of the conductivity were performed on films deposited on 5×5 mm^2 square substrates. Two parallel stripes (typical dimensions of the electrodes were 3×1 mm^2 and the distance between them around 3 mm) were painted on the surface of each sample with Ag paste (SPI supplies) to be used as electrodes, as it is shown in the inset of Figure 3. The conductances of the different substrates (purchased from Crystal GmbH) were analyzed by applying the same type of Ag contacts to bare single crystals and in the same temperature ranges as for the films.

The measurements were performed by AC impedance spectroscopy (by using a HP4192A frequency response analyzer in the range from 5 Hz−10 MHz), after letting the samples stabilize for a sufficient time at a given temperature and oxygen partial pressure (around 1 h for low temperatures, but the higher the temperature the shorter the time needed to reach a stable value of conductivity after exchanging oxygen with atmosphere). Typical impedance spectra of a film on a NGO substrate measured at different temperatures is shown in Figure 3. All films show similar behavior that can be adjusted to a simple RC circuit. The associated measured capacitance has a constant 12pF value, nondependent on measuring temperature, corresponding to the stray capacitance of the measuring setup.

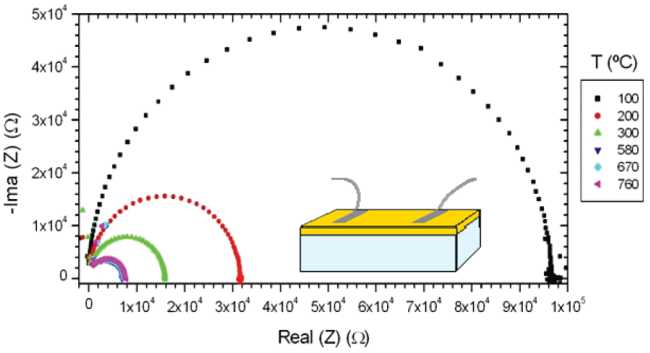

Figure 3. Schematic drawing of the silver electrodes painted on the 5×5 mm^2 thin films and impedance spectroscopy spectra for a film deposited on a NGO substrate measured at different temperatures. All films show the same behavior and could be adjusted to a simple RC circuit.

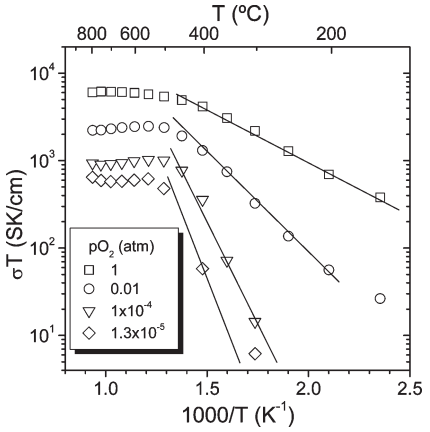

Figure 4. Planar conductivity σT versus reciprocal temperature of a 180 nm $Sr_4Fe_6O_{12+\delta}$ film deposited on NGO substrate measured at different pO_2 from 10^{-5} to 1 atm. The lines indicate the thermally activated process at T below 400 °C.

Therefore the film resistance values (contact resistance is negligible) are extracted from the intersect between the impedance arch and the real axis. The conductivity of the films was calculated assuming the current flowed homogeneously across the whole thickness of the films, and no substrate contribution was considered.

As it was explained in detail in a previous report[13] the STO and LAO substrates show similar high temperature conductances that are comparable to that of the thinner films in the high temperature range ($T > 450$ °C), so unfortunately very little information could be extracted given the difficulties to avoid the substrate contribution. However, NGO shows about 1 order of magnitude lower conductance that STO or LAO. For that reason all the conductivity analysis with pO_2 at high temperatures have been performed only in films grown on NGO substrates, with negligible contribution of the substrate to the total conductivity. The large activation energies of all substrates in comparison with films make their conductance to reduce considerably at temperatures below 450 °C so the substrate contribution becomes negligible, and therefore film conductivities are directly extracted from total conductances.

Results and Discussion

Figure 4 shows the temperature dependence (during cooling) of the conductivity of a 180 nm thick epitaxial

$Sr_4Fe_6O_{12+\delta}$ film deposited on NGO, measured at a series of different pO_2's. The logarithm of the conductivity is observed to be linear with $1/T$ at lower temperatures up to ~400 °C, as expected for a thermally activated process, making it possible to estimate an activation energy E_a and a pre-exponential factor A, from eq 1. Above a temperature of about 400−500 °C, the conductivity, at any pO_2, no longer exhibits a simple thermally activated process, but rather begins to saturate. Such saturation effects, and even decreases in conductivity at elevated temperatures, as observed here, have been reported in other mixed valence oxides and are sometimes ascribed to p-type carrier concentration depletion as the films begin losing oxygen at elevated temperatures.[20] Since the study of both temperature regimes should provide complementary information, they will each be treated in the following sections.

Transport Properties up to 400 °C. Figure 5 shows the extracted values of the activation energy E_a, for films with different thickness and grown on different substrates, plotted against log pO_2. Despite the scatter in E_a values, all specimens exhibit similar behavior regardless of the type of substrate and film thickness. E_a values strongly increase with reducing pO_2, ranging from ~0.2−0.4 eV at 1 atm to ~1.0 eV at 10^{-4} atm of O_2. In this lower temperature regime, no oxygen exchange with the atmosphere is expected, and consequently the oxygen stoichiometry of the films should depend on the equilibrium state attained at the higher temperatures at the different pO_2's. The observed increase in E_a at lower pO_2 must thus be related to a progressive reduction in the oxygen content of $Sr_4Fe_6O_{12+\delta}$. Such observations have been reported previously for p-type $Sr_4Fe_6O_{12+\delta}$ [21] bulk samples. In those cases, the increase in E_a has been related to the progressive reduction of Fe^{3+} to Fe^{2+}. One possible explanation is that this induces greater carrier localization, thereby increasing the energy barrier for polaron diffusion. Alternative explanations relate to the movement of the Fermi energy toward midgap and the consequent increase in the carrier ionization energy.

Figure 6 shows the dependence of the pre-exponential factor A, derived for the same previous group of samples, versus pO_2 in a log−log scale. One observes a power dependence that is approximately $A \propto pO_2^{-1}$ with A varying by about 4 orders of magnitude over the measured pO_2 range. At high pO_2, the larger scattering in values of A is related to the fact that these data included samples with a wider range of thicknesses. Figure 7 shows the variation of the conductivity of a series of films with different thickness deposited on NGO substrates and measured at 1 atm O_2. The conductivity is seen to increase by about an order of magnitude as the film thickness decreases from 340 to 10 nm. In Figures 8 and 9, the activation energy E_a and preexponential factor A, obtained from the low temperature regime, are shown

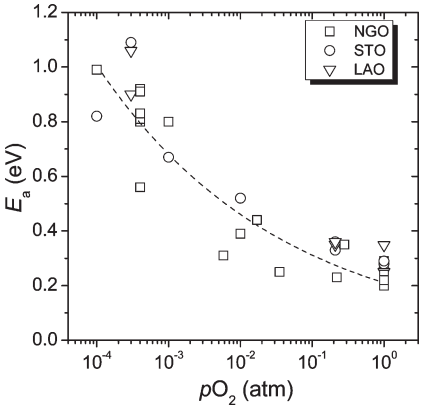

Figure 5. Activation energy E_a variation with pO_2 for films with different thickness and grown on different substrates.

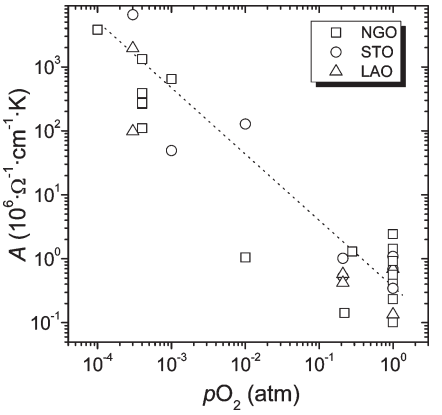

Figure 6. Pre-exponential factor A variation with pO_2 for films with different thickness and grown on different substrates.

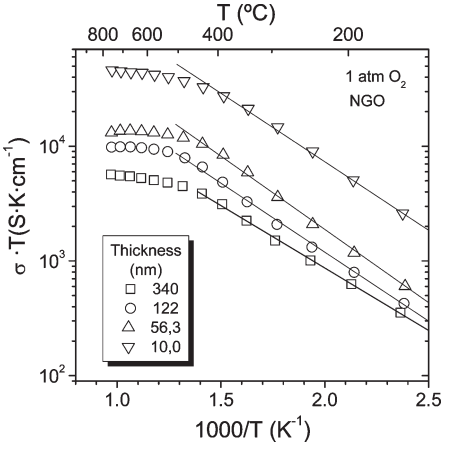

Figure 7. Planar conductivity σT versus reciprocal temperature of $Sr_4Fe_6O_{12+\delta}$ films with different thicknesses, deposited on NGO substrate, measured at 1 atm pure O_2. The lines indicate the thermally activated process at T below 400 °C.

plotted versus film thickness for films deposited on different substrates. As a general trend, Figure 8 shows that E_a decreases with increasing thickness, with the thickest films converging on the same value of E_a of approximately 0.20 eV, independent of substrate. On the other hand, the thinner films (e.g., ~20−30 nm thick) exhibit a scattering of E_a values ranging from ~0.25 to 0.35 eV. In fact, the graph suggests a region where the

(20) Menesklou, W.; Schreiner, H. J.; Hardtl, K. H.; Ivers-Tiffee, E. *Sens. Actuators, B* **1999**, *59*, 184–189.
(21) Ma, B.; Balachandran, U.; Hodges, J. P.; Jorgensen, J. D.; Miller, D. J.; Richardson, J. W., Jr. *Mater. Lett.* **1998**, *35*, 303–308.

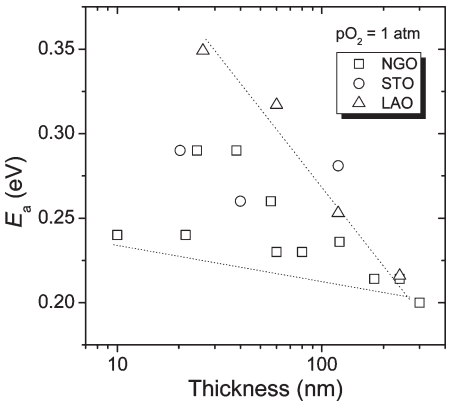

Figure 8. Activation energy E_a variation with thickness for films grown on different substrates at 1 atm O_2. The dashed lines indicate the limits for maximum and minimum E_a values. Note that the minimum values are obtained for films deposited on NGO, whereas the maximum values correspond mainly to films on LAO.

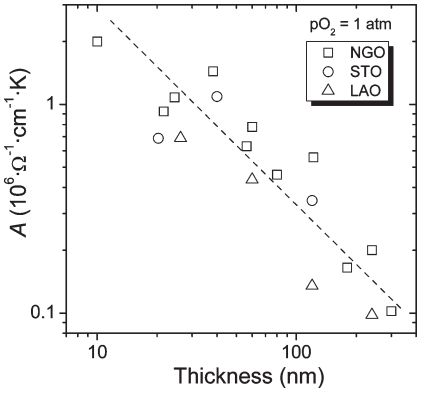

Figure 9. Pre-exponential factor A variation with thickness for films grown on different substrates at 1 atm O_2.

maximum E_a values were obtained for films deposited on LAO, whereas the minimum ones correspond to films grown on NGO. Between those limits there are intermediate values corresponding to films deposited either on NGO or STO substrates. The substrate type clearly has an influence on E_a. Figure 9 illustrates the dependence of A on film thickness, with A decreasing more than an order of magnitude, as the thickness increases from 10 to 300 nm. While in all of these films, the observed changes in E_a and A with thickness are rather small compared with changes induced by pO_2, the observed trends suggest that the differences in film thickness may have associated with them a slight variation in the overall oxygen content. Note that both the magnitude of A and E_a increase when reducing film thickness from 300 to 30 nm at constant pO_2 of 1 atm; consistent with an equivalent change of about 1 order of magnitude in pO_2. This suggests the possibility that the thinner the film, the lower its oxygen content. Despite the fact that it would seem much easier to oxidize a thin film of a few nanometers compared to a thicker film of several hundred nanometers, one cannot neglect the possible role of strain in influencing oxygen incorporation into the film. As reported in previous studies, thinner epitaxial films are generally more strained, with a typical strain (ε) dependence on thickness (t) given by $\varepsilon \propto t^{-1}$.[12] The fact that Figure 9 shows a similar dependence,

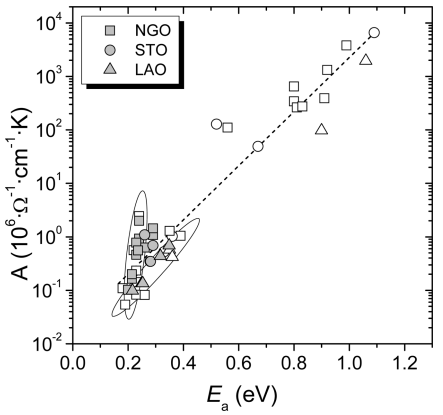

Figure 10. Correlation between pre-exponential factor A and activation energy E_a for films grown on different substrates and measured at different pO_2 (open symbols). The dashed line is a guide to the eye following the average linear dependence. The gray symbols correspond to the films with different thickness measured at 1 atm O_2. The elliptic areas correspond to the maximum and minimum E_a values in Figure 8. Note that the gray symbols on LAO follow the general behavior, whereas the gray symbols on NGO deviate from it.

$A \propto t^{-1}$ (independent of substrate type), suggests a possible relationship between changes in the pre-exponential factor A and the residual strain. Compression of films along the $a-c$ planes by epitaxial strain increases the overlap of the electron orbitals of the iron and oxygen atoms, thus leading to a higher degree of covalence of the Fe−O−Fe bonds. This feature has been reported to increase the electron−hole mobility in small-polaron conductors such as $Sr_4Fe_6O_{12+\delta}$ and other strontium iron oxides [14] or doped strontium iron perovskites [22] and would therefore contribute to an increase of the pre-exponential factor A.

Given that A and E_a have both been shown to depend on pO_2 and thickness, it is reasonable to expect that there might be also be a relationship between them. Figure 10 shows log A versus E_a for the full collection of films with different thicknesses, grown on the three types of substrates and measured at different atmospheres, from 1 atm to 3×10^{-4} atm. Despite the fact that the values come from measurements performed under very different conditions, they all follow a general common trend, i.e., roughly a linear dependence between log A and E_a, indicated by the dashed line in Figure 10. The lowest A values of about $10^5\ \Omega^{-1}\ cm^{-1}\ K$ correspond to the lowest E_a values of about 0.2 eV, whereas the largest A values of $10^{10}\ \Omega^{-1}\ cm^{-1}\ K$ correspond to E_a values above 1 eV. This dependence mainly corresponds to the pO_2 variation over the samples (empty symbols). This phenomenon is a common observation for a wide variety of activated processes, and it is known as the "compensation law" or "Meyer-Neldel rule".[23,24] There is a considerable controversy over the origin of this effect[25−29] with no

(22) Patrakeev, M. V.; Mitberg, E. B.; Lakhtin, A. A.; Leonidov, I. A.; Kozhevnikov, V. L.; Kharton, V. V.; Avdeev, M.; Marques, F. M. B. *J. Solid State Chem.* **2002**, *167*, 203–213.
(23) Constable, F. H. *Proc. Royal Soc. London, Ser. A* **1925**, *108*, 355–378.
(24) Meyer, W.; Neldel, H. *Z. Tech. Phys.* **1937**, *18*, 588–593.
(25) Yelon, A.; Movaghar, B. *Phys. Rev. Lett.* **1990**, *65*, 618–620.
(26) Wu, X.; Zheng, Y. -F. *Appl. Phys. Lett.* **2005**, *87*, 252116.
(27) Yelon, A.; Movaghar, B.; Branz, H. M. *Phys. Rev. B* **1992**, *46*, 12244–12250.

agreement on a microscopic explanation of the phenomena. However, one could use this empirical relationship as a means of detecting any deviations from this behavior. Figure 10 also contains several series of data from films with different thickness on different substrates measured in 1 atm pure O_2 (filled-in symbols). The data corresponding to films deposited on LAO show the same dependence as for the overall pO_2 variation, whereas films on NGO clearly deviate from the common trend. This is to be expected given the variations in E_a versus film thickness for the different substrates in Figure 8, with little corresponding deviations in log A vs film thickness in Figure 9.

In an attempt to find a general empirical expression for the conductivity dependence for all samples, one might assume an energy $\Lambda_0 = kT_0$ and a conductance σ_0, as characteristic parameters for a particular material or family of materials following the same activated process. Taking into account the observed relationship between log A and E_a we could rewrite the expression for the temperature dependence of the conductivity (1) as

$$\sigma T = (\sigma_0 T_0) \exp\left[-E_a\left(\frac{1}{kT}-\frac{1}{kT_0}\right)\right] \qquad (2)$$

where the expression for the pre-exponential factor is

$$A = (\sigma_0 T_0) \exp(E_a/kT_0) \qquad (3)$$

According to eq 2, the conductivity curves σT converge in a constant value ($\sigma_0 T_0$) at a characteristic temperature (T_0), called an isokinetic point. The existence of this isokinetic point means, for some authors,[29] the validity of the above-mentioned compensation law.

From the slope of the log A versus E_a in Figure 10, one extracts a common isokinetic temperature T_0 = 730(±130) °C for all samples. At this temperature all curves following the same log A versus E_a dependence should converge to a common $\sigma_0 T_0$ value, although this is not reached due to the depletion in the carrier density at high temperatures. Since the samples deviating from the general trend at 1 atm pure O_2 in Figure 10 still show the common slope when reducing the pO_2, which means a common T_0 value, they are assumed to have a different intercept (log$\sigma_0 T_0$). This σ_0 value could be thought of as corresponding to an intrinsic parameter of the $Sr_4Fe_6O_{12+\delta}$ compound related with the hypothetical maximum value that the conductivity may reach if there was no energy barrier for diffusion.

The most important differences causing variations in σ_0 correspond to those already observed in the E_a versus thickness variations plotted in Figure 8. These rely on the substrate type and very likely would correspond to the particular strain differences related to the modulated structure observed for those films,[13,17] described by a characteristic α modulation parameter. Therefore, it is possible to plot the extrapolated σ_0 values (from the intercept in Figure 10, assuming a constant slope with

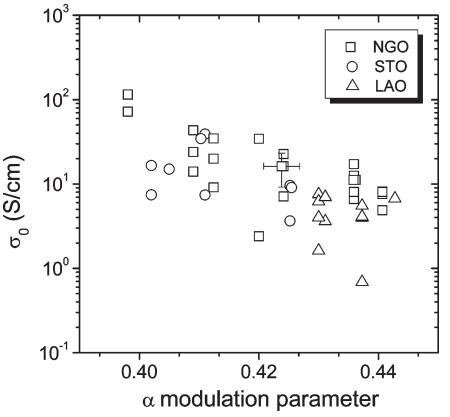

Figure 11. Dependence of the reduced conductivity σ_0 on the α modulation parameter corresponding to $Sr_4Fe_6O_{12+2\alpha}$ films obtained on different substrates.

T_0 = 730 °C for all the samples) in terms of the α modulation parameter, as shown in Figure 11 for films with different thickness and grown on different substrates. One observes that log σ_0 increases with decreasing α. The values range from $\sigma_0 \sim 1-10$ S/cm for films with the highest $\alpha \sim 0.44$ (the thickest films on NGO and STO and all the films on LAO, with the lowest epitaxial strain) as it would correspond to the equilibrium structure, up to $\sigma_0 \sim 100$ S/cm for the films with the lowest $\alpha \sim 0.40$ (the thinnest films on NGO that show the larger strain). This observation supports the hypothesis that variations in structure modulation, induced by epitaxial strain, modify the conduction mechanism. This is also consistent with the idea of considering $Sr_4Fe_6O_{12+\delta}$ as a family of $Sr_4Fe_6O_{12+2\alpha+z}$ compounds with α varying in a continuous range from 0.4 to 0.45, where each member with different α value has a different intrinsic behavior. If we compare films with constant thickness but different α values, such as the thinner films of about 20 nm in Figures 8 and 9, we observe that the change in α between films grown on the different substrates does not cause any substantial modifications in A, whereas E_a values decrease from 0.35 to 0.25 eV. The subtle oxygen changes associated with the α variation would have varied both A and E_a, following the same trend of Figures 5 and 6, so their effect in conductivity is compensated. This suggests that the modulation parameter α directly affects the activation enthalpy. The fact that the enthalpy is reduced (without affecting the A factor) is the reason for the increase of the conductivity by more than 1 order of magnitude.

Conductivity Dependency on pO_2 at High Temperatures. At temperatures above 400 °C, there is a reduction in the electrical conductivity with decreasing pO_2 (see Figure 4) due to a depletion in the majority holes as the films lose oxygen. Because the films have reached thermodynamic equilibrium at the elevated temperatures, at the different pO_2's, it is then possible to extract information from the conductivity data about the defect equilibria, and with complementary information (e.g., thermoelectric power or thermogravimetric data), the carrier transport mechanisms. Although the transport mechanism in this kind

(28) Viscor, P. *Phys. Rev.B* **2002**, *65*, 077201.
(29) Yelon, A.; Movaghar, B. *Phys. Rev. B* **2002**, *65*, 077202.

Table 1. Listing of the Key Defect Reactions, Corresponding Mass Action Relations, and the Electroneutrality Equation

defect reaction	mass action relation
$e_{vb} + h_{cb} \leftrightarrow e_{cb}{}' + h_{vb}{}^{\bullet}$ (4)	$np = K_I = N_C N_V \exp(-E_g/kT)$ (5)
	$N_{C,V} = 4.82 \cdot 10^{15} \cdot (m^*_{e,h}/m_0)^{3/2} \cdot T^{3/2}[\mathrm{cm}^{-3}]$ (6)
$O_O + V_i \leftrightarrow V_O{}^{\bullet\bullet} + O_i{}''$ (7)	$[V_O{}^{\bullet\bullet}][O_i{}''] = K_{AF} = K_{AF}{}^0 \exp(-\Delta H_{AF}/kT)$ (8)
$O_O \leftrightarrow V_O{}^{\bullet\bullet} + 2e_{cb}{}' + \frac{1}{2}O_2$ (9)	$[V_o{}^{\bullet\bullet}] n^2 p O_2^{1/2} = K_R = K_R{}^0 \exp(-\Delta H_R/kT)$ (10)
$\frac{1}{2}O_2 + V_O{}^{\bullet\bullet} \leftrightarrow O_O + 2h_{vb}{}^{\bullet}$ (11)	$p^2/[V_O{}^{\bullet\bullet}] p O_2{}^{1/2} = K_{OX} = K_{OX}{}^0 \exp(-\Delta H_{OX}/kT)$ (12)
Electroneutrality Equation	
	$n + 2[O_i{}''] + [A'] = p + 2[V_O{}^{\bullet\bullet}] + [D^{\bullet}]$ (13)

of materials is considered to correspond to small-polaron hopping, it is still possible to find evidence of a band gap between valence and conduction bands. Small polaron hopping is a result of carriers with low carrier mobility (narrow valence or conduction band) interacting with a polarizable lattice which self-traps the carrier within a potential well within the band. So, for example, if the material has shallow oxygen vacancy donors, the ionized electrons within the conduction band will exhibit a hopping energy in addition to any ionization energies. Similarly for electrons and holes generated by excitation across the band gap, those carriers will exhibit a conductivity with a temperature dependence which includes both $E_{gap}/2$ plus a hopping energy (see also relevant discussion in ref 33). Following the development of the defect model in ref 11 we list the following key defect reactions in Table 1. The first reaction corresponds to intrinsic thermal generation of conduction band electrons (e_{cb}') and valence band holes ($h_{vb}{}^{\bullet}$) from valence band electrons (e_{vb}) being excited into empty conduction band states (h_{cb}). The np product then is given in the mass action relation in terms of the conduction and valence band density of states $N_{C,V}$, which in turn depends on the electron and hole effective masses $m_{e,h}$*, and the band gap energy E_g. The second reaction corresponds to intrinsic thermal generation of oxygen Frenkel pairs made up of doubly charged oxygen vacancies ($V_O{}^{\bullet\bullet}$) and interstitials ($O_i{}''$) by moving a normal oxygen ion (O_O) into a normally empty interstitial site (V_i). The third reaction corresponds to a reduction reaction in which a normal oxygen ion leaves the lattice for the gas phase leaving behind a doubly charged oxygen vacancy and two conduction band electrons. The fourth reaction corresponds to an oxidation reaction in which oxygen from the gas phase enters the lattice by filling an oxygen vacancy and becomes doubly negatively charged by creating holes in the valence band. The fourth reaction is only added as a convenience (see below) since it is not an additional independent reaction. Finally, the last expression relates to the requirement that the solid remain overall neutral and so the sum of all negative charges on the left must equal the sum of all the positive charges on the right. In addition to oxygen vacancies ($V_O{}^{\bullet\bullet}$) and interstitials ($O_i{}''$), introduced by the anion Frenkel disorder, the defect model must also take account of all intentional and unintentional acceptor and donor impurities designated by [A'] and [$D^{\bullet}$], respectively.

When the oxygen disorder is high and fixed $[V_O{}^{\bullet\bullet}]_0$, either due to impurities (e.g., $2[V_O{}^{\bullet\bullet}]_0 \approx [A']$) or a high intrinsic ionic disorder (e.g., $[V_O{}^{\bullet\bullet}]_0 \approx K_{AF}{}^{1/2}$), then one can solve for n by substituting $[V_O{}^{\bullet\bullet}]_0$ for $[V_O{}^{\bullet\bullet}]$ in eq 10 to obtain

$$n = K_R^{1/2} [V_O^{\bullet\bullet}]_0^{-1/2} p O_2^{-1/4} \quad (14)$$

and then substitute that solution into eq 5 to solve for p as

$$p = K_I K_R^{-1/2} [V_O^{\bullet\bullet}]_0^{1/2} p O_2^{+1/4} \quad (15)$$

Equivalently, we could use eq 12 directly to solve for the hole concentration and this is given by

$$p = K_{OX}^{1/2} [V_O^{\bullet\bullet}]_0^{1/2} p O_2^{+1/4} \quad (16)$$

On the other hand, at very low $p\mathrm{O}_2$, one expects the reduction reaction to control and the electroneutrality equation can be approximated by $n = 2[V_O{}^{\bullet\bullet}]$, then solving for n with the help of eq 10, we obtain

$$n = (2K_R)^{1/3} p O_2^{-1/6} \quad (17)$$

Figure 12 shows the electrical conductivity plotted as a function of $p\mathrm{O}_2$, in a log−log plot, measured over a much

(30) Bredesen, R.; Norby, T.; Bardal, A.; Lynum, V. *Solid State Ionics* **2000**, *135*, 687–697.
(31) Patrakeev, M. V.; Mitberg, E. B.; Leonidov, I. A.; Kozhevnikov, V. L. *Solid State Ionics* **2001**, *139*, 325–330.
(32) Patrakeev, M. V.; Leonidov, I. A.; Kozhevnikov, V. L.; Kharton, V. V. *Solid State Sci.* **2004**, *6*, 907–913.
(33) Tuller, H. L. In *Oxygen Ion and Mixed Conductors and their Technological Applications* NATO Advanced Study Institute Series, Tuller, H. L., Schoonman, J., Riess, I., Eds.; Kluwer Acad. Publ. Ser.: 2000; Vol. *368*, pp 57−74.

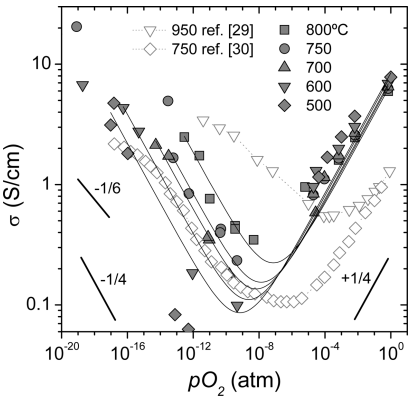

Figure 12. Isothermal conductivity variations with pO_2, at elevated temperatures of a 240 nm film. Bulk values are also shown for comparison.[30,31] Solid lines correspond to the best fit to the experimental values for each temperature assuming power dependence with ±1/4 slope for *p*- and *n*-type conductivities.

wider pO_2 range, at different temperatures (from 500 to 800 °C) for a 240 nm film deposited on NGO. For comparison, similar data reported for bulk ceramic samples are included.[30,31] At high pO_2, from 10^{-5} atm to 1 atm, the film conductivity shows a linear dependence with a slope close to the theoretically predicted +1/4 corresponding to *p*-type conductors - see eq 15 or 16. Measurements performed on other films showed a similar trend. The higher conductivity of the films, by about an order of magnitude than the reported bulk values, is likely related to the fact that in the films, transport takes place along the *a*-*c* plane of the structure, thus reflecting the anisotropy of the material, rather than the lower average value for bulk polycrystalline samples. As the pO_2 decreases ($pO_2 < 10^{-5}$ atm), the conductivity exhibits a change in slope and thereby a minimum in conductivity at intermediate pO_2. Extrapolation of the observed dependencies in the higher and lower pO_2 regions indicates that the conductivity minimum moves to higher pO_2 value with increasing T in a manner similar to that reported for bulk samples. At low pO_2, between 10^{-8} atm and 10^{-14} atm, the conductivity data show a slope of about −1/4 in pO_2 dependence, typical for *n*-type electronic conductivity (see eq 14), while at $pO_2 < 10^{-14}$ atm, the slope tends to −1/6 (see eq 17), or even lower. The −1/6 slope, corresponding to an intrinsic regime, dominated by the formation of oxygen vacancies and electrons, has been observed in bulk samples in the same extreme range of low pO_2.[22]

Since the film conductivity represents the summation of contributions from electrons, holes, and ions, and the assuming that the electronic contributions exhibit a $pO_2^{\pm 1/4}$ dependence while the ionic conductivity is independent of oxygen partial pressure ($[V_O^{\bullet\bullet}] = [V_O^{\bullet\bullet}]_0$), then we can express the overall conductivity as

$$\sigma_{tot} = \sigma_e + \sigma_{ion} + \sigma_h = \sigma_n^0 pO_2^{-1/4} + \sigma_{ion} + \sigma_p^0 pO_2^{+1/4} \quad (18)$$

with $\sigma_{n,p}^0$ being the extrapolated electronic or hole conductivity, respectively, at $pO_2 = 1$ atm and assuming pO_2 independent mobilities.

When trying to adjust the experimental data to expression 18, an optimal fit is achieved by assuming a negligible ionic contribution, i.e., $\sigma_{ion} = 0$. Although the presence of ionic conductivity in this material could not be completely ruled out, it appears to be much lower than that of the predominant electronic conductivities, over the whole pO_2 region analyzed. Fitting curves for the different temperatures are also depicted in Figure 12. Values obtained for $\sigma_{n,p}^0$ from the fitting routine for each temperature are plotted in Figure 13 as a function of reciprocal temperature. In the *p*-type region, at higher pO_2, the conductivity is mainly due to holes, and σ_p^0 is found to exhibit a weak temperature dependence with an activation energy $E_{\sigma,h}$ of −0.064 (0.006) eV as illustrated in Figure 13*a*. The activation energy for *p*-type conduction should, taking into account eq 16, be given by

$$E_{\sigma,h} = \frac{\Delta H_{ox}}{2} + E_{\mu,h} \quad (19)$$

in which $E_{\sigma,h}$ is the hopping energy for holes and ΔH_{ox} is the oxidation enthalpy. This small value of $E_{\sigma,h}$ is presumably due to the compensation of the expected temperature-activated transport mechanism, counterbalanced by the loss of electronic holes due to loss of oxygen to the atmosphere upon heating. Assuming a polaron hopping activation enthalpy $E_{\mu,h}$ of about 0.17 eV, extracted from the thicker film data obtained in the lower temperature region in Figure 7, we can extrapolate an oxidation enthalpy ΔH_{ox} of -0.47 ± 0.10 eV.

Similarly, the temperature dependence of σ_n^0 is shown in Figure 13b. The activation energy for *n*-type conduction $E_{\sigma,e}$ should, taking into account eq 14, be given by

$$E_{\sigma,e} = \frac{\Delta H_{red}}{2} + E_{\mu,e} \quad (20)$$

in which $E_{\mu,e}$ is the hopping energy for electrons, and ΔH_{red} is the enthalpy for oxygen reduction. In this region, some authors maintain that the carrier mobility in $Sr_4Fe_6O_{12+\delta}$ does not depend on temperature,[32] so we can assume $E_{\mu,e} = 0$. From the calculated slope in Figure 13 of 0.71(0.12) eV, it is thus possible to extract an enthalpy for oxygen reduction ΔH_{red} of 1.42(±0.2) eV.[33] This can be compared with a value of 1.05 eV, reported from theoretical studies,[34] and a much larger value of 3 eV, reported for bulk ceramic samples.[32] A rough value of the gap could be calculated by noting that $E_{gap} = (\Delta H_{red} + \Delta H_{ox})/2 = 0.48$ eV.

It is also possible to extract the energy gap by plotting the minimum in the electronic conductivity obtained from the conductivity-pO_2 dependence versus reciprocal temperature.[12,35,36] Since the total electronic conductivity in a semiconductor is given by $\sigma = \sigma_e + \sigma_h = ne\mu_e + pe\mu_h$, the minimum conductivity σ_{min} corresponds to the point where the extrapolation from the *n*- and *p*-type

(34) Fisher, C. A. J.; Islam, M. S. *J. Mater. Chem.* **2005**, *15*, 3200–3207.
(35) Choi, G. M.; Tuller, H. L.; Goldschmidt, D. *Phys. Rev. B* **1986**, *34*, 6972–6979.
(36) Choi, G. M.; Tuller, H. L. *J. Am. Ceram. Soc.* **1988**, *71*, 201–205.

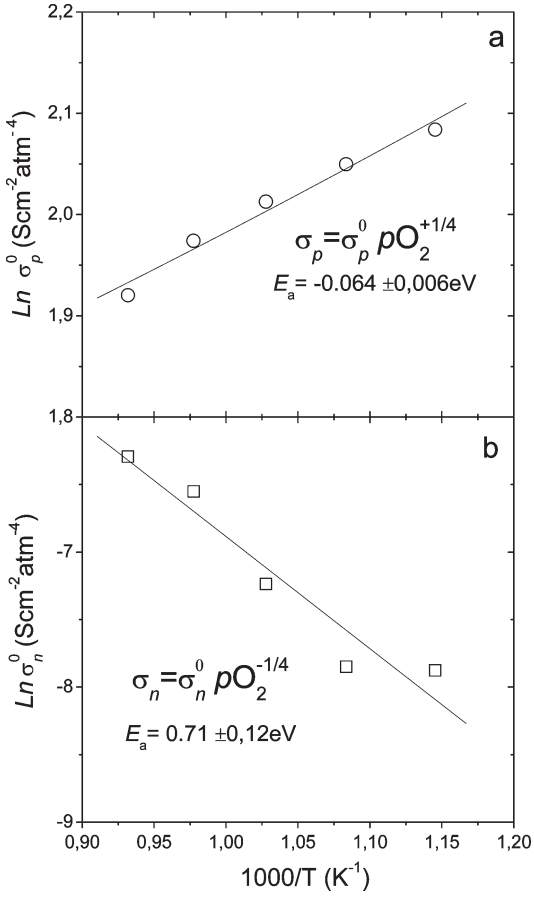

Figure 13. Dependence of reduced conductivities σ_p^0 (*a*) and σ_n^0 (*b*) (obtained from the fit curves in Figure 11) on reciprocal temperature for a 240 nm film deposited on NGO.

conductivities shows the same values $\sigma_e = \sigma_h$. Therefore

$$\sigma_{\min} = \sigma_e + \sigma_h = 2\sigma_e = 2\sigma_h = 2ne\mu_e = 2pe\mu_h \quad (21)$$

and

$$\sigma_{\min}^2 = 4pne^2\mu_e\mu_h \quad (22)$$

where p and n are the hole and electron carrier densities, respectively, e is their charge, and $\mu_{e,h}$ are their mobilities. Since the pn product can also be expressed in terms of the gap energy E_g (eq 5), the following expression is obtained in combination with 22

$$pn = N_C N_V e^{-E_g/kT} = \frac{\sigma_{\min}^2}{4e^2\mu_e\mu_h} \quad (23)$$

Then the relationship between the minimum conductivity and the gap energy is obtained as

$$\sigma_{\min} = 2e(N_C N_V \mu_e \mu_h)^{1/2} e^{-E_g/2kT} \quad (24)$$

If we assume thermally activated mobilities with energies $E_{\mu,e} = 0$ and $E_{\mu,h} = 0.17$ eV, for electrons and holes, respectively, in the analyzed range, and given that gap energy E_g depends on T as $E_g = E_g^0 - \beta T$, it is possible to obtain a value for the intrinsic gap energy

$$E(\sigma_{el,\min}) = (E_{gap}^0/2) + (E_{\mu,e} + E_{\mu,h})/2 \quad (25)$$

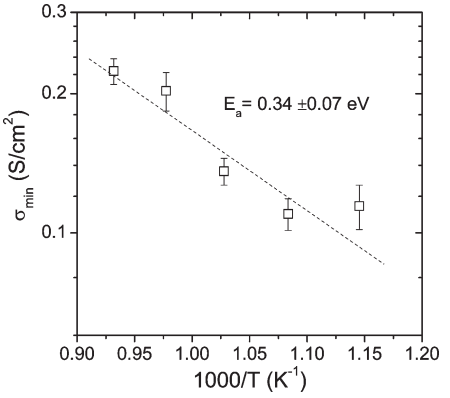

Figure 14. Dependence of the conductivity minimum $\sigma_{\min}$ versus reciprocal temperature.

directly from the slope of ln ($\sigma_{\min}$) versus reciprocal temperature $1/T$, of about $E(\sigma_{el,\min}) = 0.34$ (0.07) eV, as depicted in Figure 14, from which a value of $E_g° = 0.51 \pm 10$ eV is obtained. This value is in close agreement to the value of 0.48 eV, obtained above proving the consistency of the two methods. These values are considerably lower when compared to other related perovskites reported in the literature with $E_g°$ values between 2 and 3 eV.[11] However, there are no previously reported experimental values of the gap in $Sr_4Fe_6O_{12+\delta}$ which would allow for a direct comparison. Optical reflectivity experiments performed on 240 nm thick films showed band gap energy values of $E_g = 1.6-1.8$ eV. These optical band gap values are much larger than that estimated from the transport measurements. Significant differences can exist between a much smaller indirect thermal gap and its larger direct optical gap. Thus if $Sr_4Fe_6O_{12+\delta}$ exhibits an indirect band gap, then values obtained from photon absorption are not directly comparable to processes involving momentum transfer from phonons as in the charge transport measurements.

Conclusions

Electron hole conduction in the $Sr_4Fe_6O_{12+\delta}$ phase is thermally activated at temperatures below ~400 °C with a characteristic activation energy E_a and pre-exponential factor A. Both parameters are considerably affected by oxygen stoichiometry and film microstructure. Increasing oxygen deficiency by reduction decreases the planar conductivity in the p-type region because of a depletion of electron−hole carriers. The activation energy E_a and A at reduced temperatures increase markedly when the pO_2 at which the specimens are annealed at elevated temperatures is decreased possibly in response to higher carrier localization. The values of log A are found to increase linearly with increasing E_a, following a so-called compensation law, and, on this basis, one might define an intrinsic energy kT_o and conductivity σ_0 characteristic of electronic charge transport in $Sr_4Fe_6O_{12+\delta}$, valid for any given oxygen stoichiometry. Only the subtle variations in the modulated structure observed in this material, induced by the epitaxial strain, modify this compensation law. The reduction in the modulation periodicity, induced by the

increasing compressive strain in epitaxial films, enhances the intrinsic σ_0 value by about 1 order of magnitude, with little modification of kT_o. This may be explained by an increased overlap of the iron and oxygen electron orbitals due to compression of the films along the $a-c$ basal planes leading to a higher degree of covalence of the Fe−O−Fe bonds. This further suggests that epitaxial strain can be used in a complementary fashion to the currently used method of aliovalent doping in fundamental studies of charge transport in complex transition metal oxides as well as enabling the tailoring of their mixed electronic-conductivities.

The low temperature dependence of conductivity is correlated with the thermodynamic equilibrium attained at higher temperatures. Reduction (ΔH_R) = 1.43 eV) and oxidation enthalpies ($\Delta H_{OX} = -0.47$ eV) were successfully extracted by application of appropriate defect expressions to the temperature and pO_2 dependent electrical conductivity. A thermal band gap energy of $E_g^\circ \sim 0.5$ eV was obtained from an analysis of the temperature dependence of the conductivity minimum. This differed considerably from the optical band gap energy of about $E_g = 1.6-1.8$ eV, pointing to an indirect band gap in this material.

Acknowledgment. This work was partially supported by the MAT 2005-02601 and MAT 2008-04935 projects of the Spanish government and the SRG2005-909 project from regional government. C.S. acknowledges financial support from a FPI grant for a short stay at MIT. H.L.T. and W.J. thank the National Science Foundation Material World Network collaboration under grant numbers DMR-0243993 and DMR-0908627 and the Samsung Scholarship Foundation for partial financial support.